# Analysis of the Photoacoustic Detector Signal for Thermal Diffusivities of Gases<sup>1</sup>

J. Soldner<sup>2,3</sup>, K. Stephan<sup>2</sup>

<sup>&</sup>lt;sup>1</sup> Paper presented at the Thirteenth Symposium on Thermophysical Properties, June 22-27, 1997, Boulder, Colorado, U.S.A.

<sup>&</sup>lt;sup>2</sup> Institut für Technische Thermodynamik und Thermische Verfahrenstechnik, Universität Stuttgart, Pfaffenwaldring 9, 70569 Stuttgart, Germany

 $<sup>^{3}</sup>$  To whom correspondence should be addressed.

ABSTRACT

A resonant and a non-resonant photoacoustic detector were used to determine

thermal diffusivities of gases. With a non-resonant detector thermal diffusivities

can be determined in a wide range between  $1.0 \times 10^{-3} \ m^2 s^{-1}$  and  $1.0 \times 10^{-7} \ m^2 s^{-1}$ ,

whereas experiments with the resonant detector deliver thermal diffusivities in a

range that is about a factor of 100 smaller.

As refrigerants – HFC, HCFC and hydrocarbons – are absorbants in the infrared

at a wavelength of  $3.39\mu m$ , their thermal diffusivity can be determined without the

addition of a trace gas, particularly at pressures below 0.01 MPa. At pressures above

0.1 MPa the addition of ammonia as a trace gas is recommended. The absorption

wavelength is then  $1.531\mu m$ .

A simulation model for the non-resonant photoacoustic detector is presented

for the design of a detector and for an extended error analysis.

KEY WORDS: photoacoustic, refrigerant, thermal conductivity, thermal diffusivity

#### 1. INTRODUCTION

Transport properties such as thermal conductivity and viscosity are essential quantities for heat exchanger design, and heat transfer coefficients for these apparatus are usually determined from correlations containing these properties.

This paper focuses on measurements of the thermal conductivity of gases at moderate pressures of 0.01 MPa to 1.0 MPa. As is well known, the temperature-dependent thermal conductivity  $\lambda_0$  of the dilute gas is of prime importance for the presentation of thermal conductivities with the aid of the residual concept [1], [2].

There exist a variety of methods to measure thermal conductivities. The most often applied technique is the transient hot wire method [3], [4]. Results with this method, however, become inaccurate at pressures below 0.01 MPa. Other well established methods, such as steady-state measurements with a concentric-cylinder apparatus [5] are also not applicable in the range of pressures below 0.2 MPa. In contrast the dynamic light scattering method [6] is appropriate for thermal diffusivity measurements at high pressures, where densities are above 100  $kg m^{-3}$ . An appropriate method to measure thermal diffusivities at moderate pressures is the photoacoustic technique. As shown in experiments with argon as a reference fluid, the uncertainty is below  $\pm 1 \%$  [7]. The measured thermal diffusivity  $a = \lambda/(\rho c_v)$  can be converted into the thermal conductivity with the aid of an equation of state for density  $\rho$  and isochoric heat capacity  $c_v$ .

The photoacoustic method is based on the conversion of radiation energy into an acoustic signal. In the experiments a periodically modulated laser penetrates the sample chamber — a cylindrical cell charged with the test fluid. A small part of the radiation energy is absorbed by an absorbant added to the test gas. This absorbant is added as a trace gas in small amounts in the order of some ppm, so that the thermophysical properties of the test gas are not affected. The trace gas should be a strong absorbent at the emission wavelength of the laser, so that the energy transfer between the trace gas and the test gas inside the cell provokes a

small rise in temperature of some mK and a pressure rise of about 1 Pa. As the laser beam is modulated periodically and the wall temperature of the sample cell is held constant, temperature and pressure will alternate, as well. Thus an acoustic signal, Fig. 1, is generated. It can be detected by a sensitive microphone and the thermal diffusivity of the sample gas can be determined from the time-dependent pressure rise.

Fig. 2 shows a schematic sketch of the experimental setup. A detailed description of the electric instrumentation is given elsewhere [8]. The sample chamber consists of a stainless steel tube of 1.5 mm inner diameter and 103 mm length. It is shrunk into a copper cylinder, so that a good thermal contact is attained. The copper cylinder itself is part of a thermostat keeping the wall of the sample chamber constant within  $\pm$  1 mK. The microphone can either be mounted next to the sample chamber or, as shown in Fig. 2, outside the insulation. In the first case a temperature-resistant microphone is needed. Of advantage is that the photoacoustic detector is non-resonant. When the microphone is placed outside the insulation, the sample chamber, the coupling tube and the microphone act as an acoustic resonator, and provoke damped harmonic oscillations.

Both – the non-resonant and the resonant photoacoustic detector – are studied in the next sections. The advantages and disadvantages of each design as well as their measuring ranges are discussed. As will be shown, with refrigerants the pressure range can be extended when measurements are carried out at different wavelengths.

### 2. THE NON-RESONANT PHOTOACOUSTIC DETECTOR

The temperature rise in a non-resonant photoacoustic detector is obtained from the equation of heat diffusion in an infinite cylinder

$$\rho c_v \frac{\partial T}{\partial t} = \lambda \frac{\partial^2 T}{\partial r^2} + \frac{\lambda}{r} \frac{\partial T}{\partial r} + \mathcal{A}(r, z) \tag{1}$$

with the temperature T, time t, thermal conductivity  $\lambda$ , the radial coordinate in the sample chamber r and the axial coordinate z. The heat generation  $\mathcal{A}$  depends on the intensity I(r,z) and is given for an absorptivity below  $\alpha=0.3~m^{-1}$  by a linear relationship

$$\mathcal{A}(r,z) = \alpha I(r,z). \tag{2}$$

The intensity I(r, z) of an ideal Gaussian laser beam is given by

$$I(r,z) = \frac{W}{\pi w(z)^2} exp\left(-\frac{r^2}{w(z)^2}\right),\tag{3}$$

where W denotes the radiative power of the laser and w(z) is defined as the radius where the beam intensity reaches of 1/e of its peak value. The coordinate z has its origin in the beam focus. As shown by the experiments [8] the axial profile of the beam radius w(z) can be approximated by

$$w(z) = w_0 (1 + C^*)^{1/2}, (4)$$

wherein the constants  $w_0$  and  $C^*$  are determined from measurements of the intensity distribution of the beam at various locations inside the sample chamber with the aid of a beam-scanner. The boundary conditions are constant wall temperature  $T(t, r = R, z) = T_w$ , and rotation symmetry of the coordinate system  $(\partial T/\partial r)_{t,r=0} = 0$ .

Fig. 1 shows the pressure generated by means of a periodically modulated laser beam. It becomes obvious that the pressure towards the end of a light phase has not reached its asymptotic end value, where all radiation energy absorbed by the fluid is transferred to the wall of the sample chamber. The temperature field for a given period principally depends on the end temperatures of the previous periods. After a certain number K of periods, however, the temperature fields of successive periods become identical. When such a steady periodic state is reached the temperature field is taken as initial condition for the solution of the energy equation. The number of these periods depends on the modulation frequency and the thermal diffusivity of the the gas. As an example, we obtain K=3 for argon at T=304 K,

p=0.1015 MPa and a modulation frequency of 43 Hz.

From the local temperature rise  $\Delta T(t,r,z) = T(t,r,z) - T_w$  the average temperature rise  $\Delta \overline{T}(t)$  is obtained

$$\Delta \overline{T}(t) = \frac{1}{V} \int_{0}^{V} \Delta T(t, r, z) dV$$
 (5)

where V is the volume of the sample chamber. Temperature and pressure are related through the equation of state T(p, v), with constant specific volume v = const in our case. A Taylor series expansion yields

$$\Delta \overline{T}(t) = \overline{T} - T_0 = \left(\frac{\partial \overline{T}}{\partial p}\right)_{p_0, T_0} \cdot \Delta p(t) + \dots$$
 (6)

$$\Delta \overline{T}(t \to \infty) = \Delta \overline{T}_{\infty} = \left(\frac{\partial \overline{T}}{\partial p}\right)_{p_0, T_0} \cdot \Delta p_{\infty} + \dots \quad . \tag{7}$$

Neglecting terms of higher than first order, due to the small pressure changes, we obtain proportionality between the average temperature rise and the pressure rise

$$\frac{\Delta \overline{T}(t)}{\Delta \overline{T}_{\infty}} = \frac{\Delta p(t)}{\Delta p_{\infty}}.$$
 (8)

With Eqn. (8) and the expression for  $\Delta \overline{T}(t)$  obtained from the analytical solution of the energy equation [7], the pressure rise is

$$\Delta p(t) = \Delta p_{\infty} \left\{ 1 + \sum_{m=1}^{\infty} K_m exp\left(-\frac{\zeta_m^2 at}{R^2}\right) \times \left[ 1 - \sum_{k=1}^{K} \left\{ exp\left(-\frac{\zeta_m^2 a \left(2k-1\right)}{2R^2 f_{ch}}\right) - exp\left(-\frac{\zeta_m^2 a k}{R^2 f_{ch}}\right) \right\} \right] \right\}.$$

$$(9)$$

At the beginning of a given light phase the time is set t=0, and K is the number of previous periods.  $f_{ch}$  is the modulation frequency of the laser beam, and  $\zeta_m$  are the zeros of the Bessel function of zero order.  $K_m$  are coefficients, dependent on the beam parameters  $w_0$  and  $C^*$ , Eqn. (4).

As follows from Eqn. (9) the radius of the sample chamber should be kept as small as possible, because with increasing radius the pressure rise  $d\Delta p/dt$  decreases. As a consequence it takes more time to register the pressure rise of a light phase. This time, however, is limited by the lower cut-off frequency of the microphone. A

sample chamber with an inner diameter of 1.5 mm and a microphone with a lower cut-off frequency of 0.1 Hz permit measurements down to  $a = 1.0 \times 10^{-7} \ m^2 s^{-1}$ . The maximum modulation frequency of the laser light of 200 Hz limits the measuring range to thermal diffusivities below  $a = 1.0 \times 10^{-3} \ m^2 s^{-1}$ .

One the other hand the microphone of (1/2)" diameter is mounted next to the tube of 1.5 mm diameter, whereby a clearance volume in front of the microphone cannot be avoided entirely. Moreover, microphones are equipped with a capillary tube that equalizes the static pressure on both sides of the microphone membrane. This capillary tube is designed in such a way that the acoustic pressure is not influenced for sample volumes above  $2000 \ mm^3$ . In our case the volume of the sample chamber is  $170 \ mm^3$ . Both – the clearance volume and the mass flow in the capillary tube of the microphone – provoke changes of the density in the sample chamber during the pressure rise so that the assumption of a constant density in the Taylor series expansion, Eqns. (6) and (7), no longer holds. In order to study the influence on the the pressure rise, the mass and the energy balances were solved simultaneously, for the system according to Fig. 3. For an ideal gas, the energy equation in system 1 reads

$$\rho c_v \frac{\partial T_1}{\partial t} - \frac{\mathcal{R}T_1}{V_1} \frac{dm_1}{dt} = \lambda \frac{\partial^2 T_1}{\partial r^2} + \frac{\lambda}{r} \frac{\partial T_1}{\partial r} + \mathcal{A}(r)$$
 (10)

where  $\mathcal{R}$  denotes the specific gas constant. The average temperature is

$$\overline{T}_1(t) = \frac{1}{V} \int_0^V T_1(t, r) dV. \tag{11}$$

The gas velocities  $\omega$  in the throttles are obtained from the Bernoulli-equation

$$\frac{1}{2}\omega^2 + \int_{p_1}^{p_2} \frac{1}{\rho} dp + \frac{1}{2}\omega^2 \frac{L}{D} f = 0, \tag{12}$$

where L is the tube length, D the diameter and f the friction factor, which is for laminar flow f = 64/Re. Neglecting the compressibility of the gas and the friction in the boring, in Eqn. (12), the mass balance of system 1 yields

$$\frac{dm_1}{dt} = -\pi \frac{D_1^2}{4} \rho \omega = -\pi \frac{D_1^2}{4} \sqrt{2\rho(p_1 - p_2)} = -\pi \frac{D_1^2}{4} \sqrt{2\rho \mathcal{R} \left(\frac{m_1 \overline{T}_1}{V_1} - \frac{m_2 \overline{T}_2}{V_2}\right)}. \quad (13)$$

Under adiabatic conditions the energy and mass balances for system 2 and 3 are

$$c_v m_2 \frac{d\overline{T}_2}{dt} - (c_v + \mathcal{R}) \left( \overline{T}_2 - \overline{T}_1 \right) \frac{dm_1}{dt} - \mathcal{R} \overline{T}_2 \frac{dm_2}{dt} = 0, \tag{14}$$

$$\frac{dm_2}{dt} = -\frac{dm_1}{dt} - \frac{dm_3}{dt},\tag{15}$$

$$c_v m_3 \frac{d\overline{T}_3}{dt} - \mathcal{R}\overline{T}_3 \frac{dm_3}{dt} = 0, \tag{16}$$

$$\frac{dm_3}{dt} = \pi \frac{D_3^2}{4} \rho \omega = -8\pi \rho \nu L + \sqrt{64\pi^2 \rho^2 \nu^2 L^2 + \frac{\pi^2 \rho D^4 \mathcal{R}}{8} \left(\frac{m_2 \overline{T}_2}{V_2} - \frac{m_3 \overline{T}_3}{V_3}\right)}, \quad (17)$$

where  $\nu$  denotes the kinematic viscosity of the gas. The initial conditions are  $T_{1(t=0,r)} = T_w$ ,  $m_{i(t=0)} = p_0 V_i/(\mathcal{R}T_w)$  and  $\overline{T}_{i(t=0)} = T_w$ . As a result of a numerical solution of the differential equations (10) to (16) the state variables  $T_1(r,t)$ ,  $\overline{T}_1(t)$ ,  $\overline{T}_2(t)$ ,  $\overline{T}_3(t)$ ,  $m_1(t)$ ,  $m_2(t)$  and  $m_3(t)$  are obtained. The pressure is then obtained with the aid of the equation of state for ideal gases. The microphone signal S is

$$S = k_m k_a (p_2 - p_3) \tag{18}$$

with the amplification factor of the microphone  $k_m$ , and  $k_a$  of the amplifier. These values are tabulated in the calibration charts of the manufacturer.

The solid curve in Fig. 4 refers to the measured photoacoustic signal for argon at T=304 K and p=0.1015 MPa with 1000 ppm ethane as a trace component. The volumes of the sample chambers were  $V_1 = 177 \ mm^3$ ,  $V_2 = 543 \ mm^3$ ,  $V_3 = 334 \ mm^3$ , the absorptivity is  $\alpha = 0.17 \ m^{-1}$  and the laser power is W=5 mW. The heat generation according to Eqn. (3) was determined for an average beam radius of  $\overline{w} = 0.257mm$ . The dash-dotted curve is the result of the simulation. It agrees well with the experiments. Between 0 s and 0.018 s a considerable high mass flow from system 1 to system 2 and from system 2 to 3 provokes a density decrease in the sample chamber so that the pressure rise is lower than that according to Eqn. (9) for constant density, dashed curve. The pressure decrease after 0.018 s is caused by the mass flow in the capillary tube of the microphone. This mass flow is almost constant.

As the results clearly indicate, the clearance volume in front of the microphone

membrane has to be kept as small as possible. It should be lower than 10% of the volume of the sample chamber. Additional flow resistances between both sides of the membrane are useful to reduce the mass flow inside the microphone.

## 3. THE RESONANT PHOTOACOUSTIC DETECTOR

Fig. 2 shows the setup of an resonant photoacoustic detector. The sample chamber, the microphone chamber and the coupling tube form an acoustic resonator a so-called Helmholtz resonator. The gas in the coupling tube behaves as if it were moved as a plunger towards one chamber and thus compresses the gas there, whereas the gas in the other chamber expands. The pressure difference between both chambers provoke a counter-acting force accelerating the plunger in the inverse direction. The oscillation thus generated is damped due to the friction of the wall. The damping factor  $\delta$  and the angular frequency  $\omega$  of the oscillations are [7]

$$\delta = -\frac{8\pi\eta}{A\rho} \qquad \omega = \sqrt{\frac{Av_s^2}{L_R V_2} - \frac{16\pi^2\eta^2}{A^2\rho^2}}$$
 (19)

where  $v_s$  is the velocity of the sound,  $\eta$  the viscosity, A the cross-section and  $L_R$  the length of the coupling tube.

By means of a resonant detector, reference measurements with argon lead to an uncertainity below  $\pm$  1%, although the clearance volume in front of the microphone is greater than that of the non-resonant cell. As in the case of harmonic oscillations, the mass flows are oscillating too, but the time averaged density in the chamber remains constant. The pressure rise can be understood as a superposition of the pressure rise according to Eqn. (9) and damped harmonic oscillations. Therefore the dashed curve, Fig. 5, referring to the pressure rise according to Eqn. (9) intersects the measured curve in its inflection points.

A serious disadvantage of the resonant detector is, that accurate results are obtained only when the harmonic oscillations are not too intensively damped, otherwise density changes in the sample chamber and errors become intolerable.

#### 4. SUITABLE TRACE GASES

Previous experiments were made with argon as a test gas [7], [8] with a helium-neon laser at a wavelength of 3.39  $\mu m$ , corresponding to a wave number of 2950  $cm^{-1}$ . Around this wavelength the infrared spectra of hydrocarbons and refrigerants have strong absorption bands caused by transitions to a higher vibrational level of the C-H bond. A trace gas therefore is not needed. The pressure range, however, is limited to pressure below 0.01 MPa. Otherwise the absorbed radiation energy is too high. If the absorbed energy is above 5% of the incoming energy, axial temperature gradients cannot be neglected and thus Eqn. (9) is no longer valid. Hydrocarbons, in general, do not absorb at a wavelength of 1.531  $\mu m$ , where ammonia has a local absorption maximum with a line strength of  $S=1.85\times 10^{-21}~cm/molecule$ at T=293 K. Assuming a Lorentz profile and a line width of  $\nu = 0.1~cm^{-1}$  it is recommended to fill in ammonia with a partial pressure of at least 300 Pa in order to achieve a sufficient high absorptivity coefficient of about 0.09  $m^{-1}$ . This value leads to a photoacoustic signal, high enough, so that measurements can be carried out at pressures above 0.1 MPa without affecting the thermophysical properties of the test gas. In the intermittent pressure range between 0.01 MPa and 0.1 MPa, the ammonia added to the test gas change the thermal diffusivity, the density and the isochoric heat capacity. The errors thus introduced must be corrected.

#### 5. CONCLUSIONS

A non-resonant photoacoustic detector is an efficient measurement technique for precise measurements of thermal diffusivities in the range between  $1.0 \times 10^{-3} \ m^2 s^{-1}$  and  $1.0 \times 10^{-7} \ m^2 s^{-1}$ . Such a non-resonant cell should be preferred because measurements can be performed in a range of thermal diffusivities that is almost a factor of 100 wider than the range that can be obtained with the resonant cell.

Measurements with refrigerants at pressures below 0.01 MPa can be carried out

with a helium-neon laser at an emission wavelength of 3.39  $\mu m$ . As the refrigerants show strong absorption bands around this wavelength, a trace gas is not needed. In this pressure range the refrigerants can be considered as ideal gases so that the measured thermal diffusivities can be easily converted into thermal conductivities. Above 0.1 MPa the thermal diffusivity of refrigerants can be measured, when ammonia is added as a trace gas.

As the model clearly indicates, the clearance volume in front of the microphone should be kept below 10 % of the volume of the sample chamber. Due to the small volume of the sample chamber, the mass flow in the capillary tube connecting both sides of the membrane, should be reduced.

## REFERENCES

- V. Vesovic, W. A. Wakeham, G. A. Olchowy, J. V. Sengers, J. T. R. Watson, and J. Millat. J. Phys. Chem. Ref. Data <u>19</u>:763, (1990).
- [2] A. Laesecke, R. Krauss, K. Stephan, and W. Wagner. J. Phys. Chem. Ref. Data 19:1089, (1990).
- [3] W. A. Wakeham, A. Nagashima, and J. V. Sengers. Measurement of the transport properties of fluids. In *Experimental Thermodynamics*, Vol. III, chapter 7. Blackwells Scientific, Oxford, 1991.
- [4] B. Taxis and K. Stephan. Int. J. Thermophys. <u>15</u>:141, (1994).
- [5] Y. Tanaka, M. Nakata, and T. Makita. Int. J. Thermophys. <u>12</u>:949, (1991).
- [6] B. Kruppa and J. Straub. Fluid Phase Equil. 80:305, (1992).
- [7] J. Soldner and K. Stephan. Proceedings of the 2nd European Thermal-Sciences and 14th UIT National Heat Transfer Conference, Rome 2:1071, (1996).
- [8] J. Soldner and K. Stephan. Proceedings of the 23rd International Thermal Conductivity Conference, Nashville <u>1</u>:481 (1996).

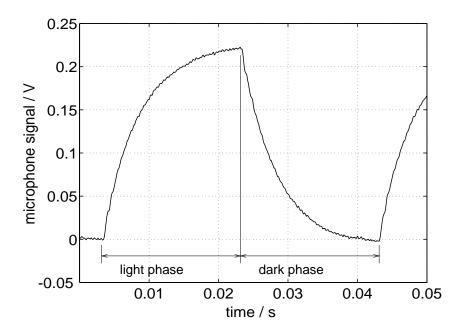


Fig. 1: The photoacoustic signal

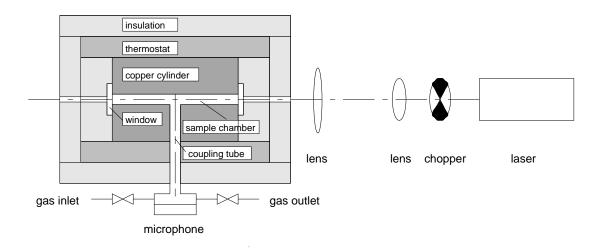


Fig. 2: The experimental setup

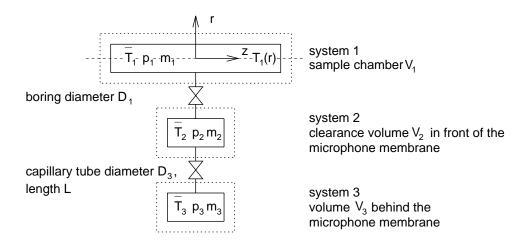


Fig. 3: The model of a non-resonant photoacoustic detector

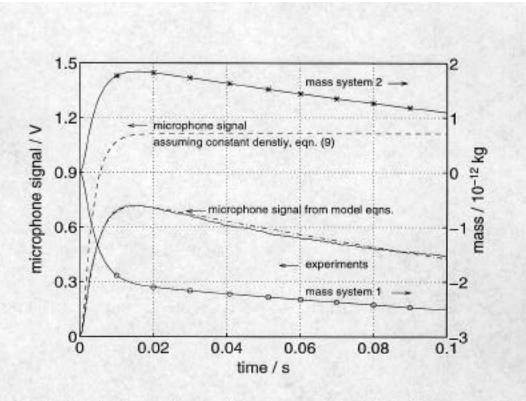


Fig. 4: The photoacoustic signal for argon at T=304 K and p=0.1015 MPa

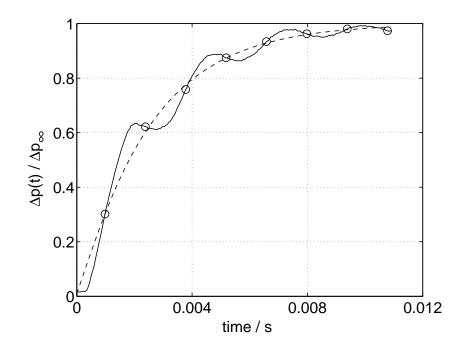


Fig. 5: Helmholtz oscillations in a resonant photoacoustic detector